JOURNAL OF GUIDANCE, CONTROL, AND DYNAMICS
Vol. 30, No. 2, March–April 2007

Near-Optimal Very Low-Thrust Earth-Orbit Transfers and Guidance Schemes

Yang Gao*
Chinese Academy of Sciences, 100080 Beijing, People's Republic of China

DOI: 10.2514/1.24836

A novel direct approach is developed for computing near-optimal very low-thrust Earth-orbit transfers and constructing feasible onboard guidance schemes for the spacecraft propelled by low-thrust acceleration with thrust-to-weight ratio on the order of 10^{-5}. Both minimum-time and minimum-fuel orbital transfers with a mechanism for coasting are solved. The direct approach employs three types of control laws—the perigee-centered tangential steering, apogee-centered inertial steering, and piecewise constant yaw steering, over different orbital arcs within each transfer revolution to simultaneously change semimajor axis, eccentricity, and inclination, respectively. An analytic orbital averaging technique is developed to efficiently propagate the long-duration, many-revolution trajectories by computing analytic incremental changes in classical orbital elements for each transfer revolution involving thrusting, and Earth J_2 and shadow effects. The optimal orbital transfer problems are converted to parameter optimization problems that are in turn solved by nonlinear programming, and only a small number of parameters related to the control laws are optimized. The onboard guidance schemes that guide the spacecraft in an open-loop fashion are developed based on optimal parameters obtained by trajectory optimization results. Finally, numerical results of Earth-orbit transfers and performances of guidance schemes are presented.

Nomenclature

a	=	semimajor axis, km
E	=	eccentric anomaly, deg
e	=	eccentricity
$e_{1,2}$	=	tangential steering angles, deg
f	=	thrust acceleration, m/s^2
f_{in}	=	in-plane thrust acceleration, m/s^2
f_n	=	out-of-plane thrust acceleration, m/s^2
f_r	=	in-plane radial thrust acceleration, m/s^2
f_θ	=	in-plane circumferential thrust acceleration, m/s^2
g	=	Earth's gravitational acceleration at sea level, 9.80665 m/s^2
h	=	specific angular momentum, m^2/s
I_{sp}	=	specific impulse, s
i	=	inclination, deg
J_2	=	Earth oblateness constant, 1082.6×10^{-6}
M	=	mean anomaly, deg
m	=	spacecraft mass, kg
n	=	averaged mean motion, rad/s
P	=	input power of solar electric propulsion, kW
R_e	=	Earth radius, 6378.145 km
r	=	orbital radius, km
$s_{1,2}$	=	inertial steering angles, deg
t	=	time, s
v	=	spacecraft velocity magnitude, km/s
$\mathbf{x}$	=	state vector of classical orbital elements, $(a, e, i, \Omega, \omega)$
$y_{1,2,3,4}$	=	constant yaw steering angles, deg
α	=	in-plane pitch angle, deg
$\tilde{\alpha}$	=	angle from velocity vector to projection of thrust vector onto orbit plane, deg
β	=	out-of-plane yaw angle, deg
γ	=	flight-path angle, deg
η	=	thruster efficiency
θ	=	true anomaly, deg
μ	=	Earth's gravitational constant, 398, 601 km^3/s^2
Ω	=	longitude of the ascending node, deg
ω	=	argument of periapsis, deg

Subscripts

en	=	Earth-shadow entrance
ex	=	Earth-shadow exit
f	=	final value
0	=	initial value

Received 27 April 2006; revision received 5 September 2006; accepted for publication 6 October 2006.

*Associate Research Fellow, Academy of Opto-Electronics, Department of Space System Engineering. P.O. Box 8701; GaoY@aoe.ac.cn.

Introduction

THE NASA Deep Space 1 and ESA SMART-1 missions have demonstrated successful uses of low-thrust solar electric propulsion (SEP) for an interplanetary mission and a lunar mission [1,2]. The utilization of low-thrust propulsion (including SEP technology) for the Earth-orbit spacecraft also has been a popular research topic. However, how to design optimal Earth-orbit transfer trajectories using SEP as the primary means of propulsion is still challenging because the thrust acceleration is much lower than the gravitational acceleration such that the transfer trajectories, unlike interplanetary transfer trajectories, usually consist of hundreds or even thousands of orbital revolutions. For example, the transfer times are usually several months for a SEP spacecraft with thrust-to-weight ratio on the order of 10^{-5} to transfer from a low Earth orbit to a geostationary orbit. Furthermore, Earth J_2 and shadow effects should be considered if the spacecraft transfers through relatively low-altitude orbits, which makes the optimal orbital transfer problem much harder to solve.

A widely used program for very low-thrust Earth-orbit transfers using SEP is SEPSPOT [3], which solves the two-point boundary value problem (2PBVP) using a shooting method. However, the solution of the 2PBVP is very sensitive to the initial guess for the costate variables that do not have intuitive physical meanings. Direct methods are also used to deal with long-duration orbital transfer problems. For example, Betts [4] used the collocation method to solve a 578-revolution transfer by nonlinear programming (NLP), leading to a sparse optimization with 416,123 variables and 249,674 constraints. To reduce the problem dimension, Scheel and Conway [5] employed a parallel Runge–Kutta method to solve planar transfers with very low thrust. However, the control steering still

requires a large number of nodes as NLP design variables. Later, Kluever [6] used a blended control law and an orbital averaging technique to solve minimum-time near-Earth orbit transfers including Earth shadow and oblateness effects. This method requires a relatively small number of design variables and employs the orbital averaging technique to speed up the numerical integration process. Ferrier and Epenoy [7] solved minimum-time transfers under the constraint of an eclipse by means of the averaging technique and a smoothing method. However, most of the early works do not consider the minimum-fuel transfers that might involve burn-coast sequences out of the Earth's shadow. Recently, Haberkorn et al. [8] developed a homotopic approach to solve fixed-time minimum-fuel orbital transfers involving hundreds of orbital revolutions in an ideal gravity field but they did not consider the shadow effects that might affect the transfers significantly. The homotopic approach was also used for solving minimum-time transfers to geosynchronous orbits [9].

This paper demonstrates a novel direct approach for solving both minimum-time and minimum-fuel (involving coasting mechanism) orbital transfer problems using very low thrust in the presence of Earth J_2 and shadow effects. Three simple control laws are employed over different orbital arcs within each orbital revolution to simultaneously change the semimajor axis, eccentricity, and inclination, respectively. The analytic incremental changes in classical orbital elements over an orbital revolution have been derived, with which the trajectory propagation time is greatly reduced while satisfactory solution accuracy is maintained. The novel approach requires only a small number of parameter optimization design variables so that the optimization process is significantly expedited. Furthermore, the control laws can be easily implemented onboard to form guidance schemes in an open-loop fashion, and only a few parameters need to be stored onboard.

Control Laws

Three control laws, tangential steering, inertial steering, and piecewise constant yaw steering, are used in this work to simultaneously change semimajor axis, eccentricity, and inclination, respectively, for each orbital revolution. The tangential steering is either along or opposite to the velocity direction, which is the most efficient strategy to change the semimajor axis instantaneously. The inertial steering is perpendicular to the semimajor axis, which is a near-optimal strategy to change eccentricity [10]. The piecewise constant yaw steering is developed to change inclination. Three types of control laws are used over different orbital arcs within each transfer revolution such that the tangential steering is used around the perigee, the inertial steering around the apogee, and the piecewise constant yaw steering at locations that are optimally chosen. The goal of these three relatively simple control laws is to change orbital energy, eccentricity, and inclination in a simple and efficient fashion.

The illustration of the proposed control strategy for each orbital revolution is shown in Fig. 1. Tangential steering is applied from s_1 to s_2, inertial steering from e_1 to e_2, and constant yaw steering from y_1 to y_2 and from y_3 to y_4. There is no thrust in the Earth's shadow, and the Earth shadow entrance/exit angles E_{en} and E_{ex} are obtained by solving a quartic problem (see [11]) in terms of the calendar date corresponding to each orbital revolution. All angular variables in Fig. 1 are evaluated in true anomaly unless otherwise stated.

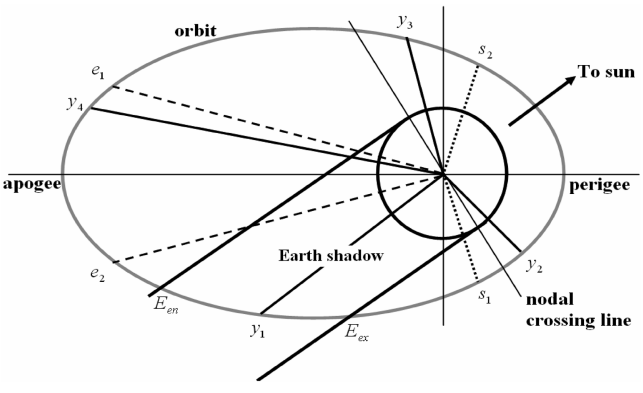

Fig. 1 Control laws employed over different orbital arcs.

It should be noted that the locations of the perigee and apogee change (i.e., the line of apsides rotates) in the inertial space during transfers due to low thrust and J_2 perturbations, and E_{en} and E_{ex} vary as well due to the Earth's rotation around the sun. In addition, the term "inertial steering" is not entirely correct because the semimajor axis is not inertially fixed, which means that the inertial steering also varies. Nevertheless this term is used throughout this paper.

The most efficient strategy to change orbital energy can be obtained from the variational form of the semimajor axis

$$\frac{\mathrm{d}a}{\mathrm{d}t} = \frac{2a^2 v}{\mu} f_{\text{in}} \cos\tilde{\alpha} \tag{1}$$

By setting $\partial(\mathrm{d}a/\mathrm{d}t)/\partial\tilde{\alpha} = 0$, we can easily obtain $\tilde{\alpha} = 0$ or $\tilde{\alpha} = \pi$ (along or opposite to the velocity direction). With $\tilde{\alpha} = 0$ or $\tilde{\alpha} = \pi$, $|\mathrm{d}a/\mathrm{d}t|$ reaches maximum value at the perigee point because the velocity amplitude at perigee is largest. Thus, the typical perigee-centered burn arc is used, and then the starting and ending points (s_1 and s_2) for the tangential steering are represented by a single parameter w_s

$$s_1 = -|w_s|\pi \tag{2}$$

$$s_2 = |w_s|\pi \tag{3}$$

where $-1 \le w_s \le 1$. Furthermore, we define the fact that the semimajor axis is increased as $0 \le w_s \le 1$, and is decreased as $-1 \le w_s < 0$.

According to [10], the inertial steering perpendicular to the semimajor axis is near optimal to change eccentricity. This steering can be expressed as $\alpha = \theta$ (or $\tilde{\alpha} = \theta - \gamma$) to reduce eccentricity and $\alpha = \pi + \theta$ (or $\tilde{\alpha} = \pi + \theta - \gamma$) to increase eccentricity. Note again that the steering is not inertial because the semimajor axis orientation (or eccentricity vector) is not fixed in space during transfers. Observe the variational form of eccentricity

$$\frac{\mathrm{d}e}{\mathrm{d}t} = \frac{f_{\text{in}}}{v}[2(e + \cos\theta)\cos\tilde{\alpha} - (r/a)\sin\theta\sin\tilde{\alpha}] \tag{4}$$

The fact that the velocity at apogee is smallest implies that the typical apogee-centered burn arc can be used to efficiently change eccentricity. Therefore, the starting and ending points (e_1 and e_2) are represented by a single parameter w_e

$$e_1 = \pi - |w_e|\pi \tag{5}$$

$$e_2 = \pi + |w_e|\pi \tag{6}$$

where $-1 \le w_e \le 1$. We define the fact that the eccentricity is increased as $0 \le w_e \le 1$ and is decreased as $-1 \le w_e < 0$.

The strategy to change inclination is the piecewise constant yaw steering around points where the inclination is most efficient to change. The same strategy is also employed by Falck and Gefert [12] for low-thrust inclination control. From the variational form of inclination,

$$\frac{\mathrm{d}i}{\mathrm{d}t} = \sqrt{\frac{p}{\mu}}\frac{\cos(\omega + \theta)}{1 + e\cos\theta} f_n \tag{7}$$

we can find the best places to change inclination with a constant out-of-plane thrust component by setting $\partial(\mathrm{d}i/\mathrm{d}t)/\partial\theta = 0$. Then, we can get

$$\sin(\omega + \theta) = -e\sin\omega \tag{8}$$

Locations where the changes of inclination are local optima can be obtained as follows:

$$\theta_1^m = \sin^{-1}(-e\sin\omega) - \omega \tag{9}$$

$$\theta_2^m = \pi - \sin^{-1}(-e\sin\omega) - \omega \tag{10}$$

Therefore, the maximum value of $|\mathrm{d}i/\mathrm{d}t|$ occurs at either θ_1^m or θ_2^m. We define another term as follows:

$$\left[\frac{\mathrm{d}i}{\mathrm{d}t}\right]_{\max} = \max\left(\left|\frac{\cos(\omega+\theta_1^m)}{1+e\cos\theta_1^m}\right|, \left|\frac{\cos(\omega+\theta_2^m)}{1+e\cos\theta_2^m}\right|\right) \tag{11}$$

We introduce a parameter $0 \le w_Y \le 1$, and let

$$\frac{\cos(\omega+\theta)}{1+e\cos\theta} = \pm w_Y\left[\frac{\mathrm{d}i}{\mathrm{d}t}\right]_{\max} \tag{12}$$

There are at last two pairs of solutions of θ (denoted by y_1 and y_2, and y_3 and y_4) for the above nonlinear equations:

$$y_1 = \psi_1, \quad y_2 = \psi_2 \quad \text{with} \quad 0 \le \psi_i \le 2\pi, \quad i = 1,2 \tag{13}$$

where

$$\begin{aligned}\psi_1 &= \cos^{-1}\left(w_Y\left[\frac{\mathrm{d}i}{\mathrm{d}t}\right]_{\max}\Big/A_1\right) - \varphi_1,\\ \psi_2 &= -\cos^{-1}\left(w_Y\left[\frac{\mathrm{d}i}{\mathrm{d}t}\right]_{\max}\Big/A_1\right) - \varphi_1\end{aligned} \tag{14}$$

$$\sin\varphi_1 = \sin\omega/A_1, \qquad \cos\varphi_1 = \left(\cos\omega - ew_Y\left[\frac{\mathrm{d}i}{\mathrm{d}t}\right]_{\max}\right)\Big/A_1 \tag{15}$$

$$A_1 = \sqrt{1 - 2e\cos\omega w_Y\left[\frac{\mathrm{d}i}{\mathrm{d}t}\right]_{\max} + \left(ew_Y\left[\frac{\mathrm{d}i}{\mathrm{d}t}\right]_{\max}\right)^2} \tag{16}$$

If there are no solutions for y_1 and y_2, let $y_1 = y_2 = \theta_i^m$ $(i = 1,2)$ and the subscript i is determined by $\cos(\omega+\theta_i^m) \ge 0$. The other pair of solutions is

$$y_3 = \psi_3, \quad y_4 = \psi_4 \quad \text{with} \quad 0 \le \psi_i \le 2\pi, \quad i = 3,4 \tag{17}$$

where

$$\begin{aligned}\psi_3 &= \cos^{-1}\left(-w_Y\left[\frac{\mathrm{d}i}{\mathrm{d}t}\right]_{\max}\Big/A_2\right) - \varphi_2,\\ \psi_4 &= -\cos^{-1}\left(-w_Y\left[\frac{\mathrm{d}i}{\mathrm{d}t}\right]_{\max}\Big/A_2\right) - \varphi_2\end{aligned} \tag{18}$$

$$\sin\varphi_2 = \sin\omega/A_2, \qquad \cos\varphi_2 = \left(\cos\omega + ew_Y\left[\frac{\mathrm{d}i}{\mathrm{d}t}\right]_{\max}\right)\Big/A_2 \tag{19}$$

$$A_2 = \sqrt{1 + 2e\cos\omega w_Y\left[\frac{\mathrm{d}i}{\mathrm{d}t}\right]_{\max} + \left(ew_Y\left[\frac{\mathrm{d}i}{\mathrm{d}t}\right]_{\max}\right)^2} \tag{20}$$

If there are no solutions for y_3 and y_4, let $y_3 = y_4 = \theta_i^m$ $(i = 1,2)$ and the subscript i is determined by $\cos(\omega+\theta_i^m) < 0$. Furthermore, we introduce a parameter $-1 \le w_A \le 1$ to represent the amplitude of the yaw steering component:

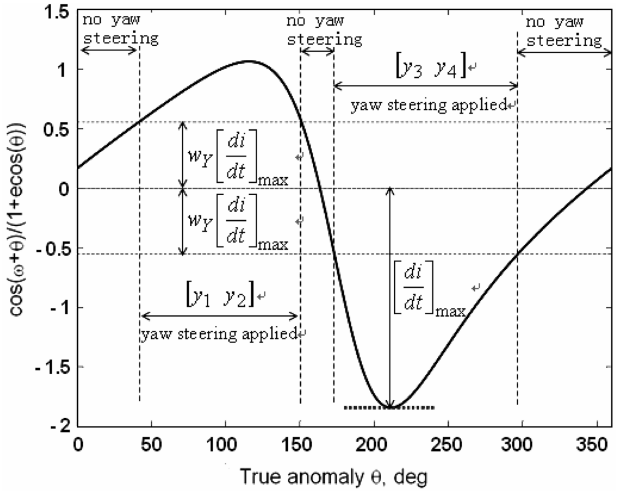

Fig. 2 Illustration of yaw steering ($e = 0.7$, $\omega = 5$ rad).

$$f_n = \begin{cases} fw_A & \text{if } \theta \text{ is between } y_1 \text{ and } y_2\\ -fw_A & \text{if } \theta \text{ is between } y_3 \text{ and } y_4\\ 0 & \text{otherwise}\end{cases} \tag{21}$$

The parameter w_A is related to the yaw steering angle β by $w_A = \sin\beta$ or $\beta = \sin^{-1}w_A$. Note that the inclination is defined to increase as $0 \le w_A \le 1$ and decrease as $-1 \le w_A < 0$. The yaw steering within one orbital revolution is illustrated in Fig. 2.

Parameters to describe the orbital arcs, on which three different control laws are employed, have been defined. These parameters are $w_s \in [-1 \quad 1]$ for the tangential steering, $w_e \in [-1 \quad 1]$ for the inertial steering, and $w_Y \in [0 \quad 1]$ and $w_A \in [-1 \quad 1]$ for the constant yaw steering. These three control laws are relatively simple and expected to change orbital energy, eccentricity, and inclination in an efficient way within each orbital revolution. In the following section, the analytic orbital averaging technique is developed to propagate the many-revolution transfer trajectories using the proposed control laws.

Analytic Orbital Averaging Technique

Because precisely integrating long-duration, slowly developing spiral trajectories is computationally time consuming, the analytic orbital averaging technique is used to significantly reduce the computation load in this work. We start with the Gauss' variational equations (22–27) [13]:

$$\frac{\mathrm{d}a}{\mathrm{d}t} = \frac{2a^2e\sin\theta}{h}f_r + \frac{2a^2p}{hr}f_\theta \tag{22}$$

$$\frac{\mathrm{d}e}{\mathrm{d}t} = \frac{1}{h}p\sin\theta f_r + \frac{1}{h}[(p+r)\cos\theta + re]f_\theta \tag{23}$$

$$\frac{\mathrm{d}i}{\mathrm{d}t} = \frac{r\cos(\omega+\theta)}{h}f_n \tag{24}$$

$$\frac{\mathrm{d}\Omega}{\mathrm{d}t} = \frac{r\sin(\omega+\theta)}{h\sin i}f_n \tag{25}$$

$$\frac{\mathrm{d}\omega}{\mathrm{d}t} = -\frac{p\cos\theta}{he}f_r + \frac{(p+r)\sin\theta}{he}f_\theta - \frac{r\sin(\omega+\theta)\cos i}{h\sin i}f_n \tag{26}$$

$$\frac{\mathrm{d}M}{\mathrm{d}t} = n + \frac{1}{a^2 ne}[(p\cos\theta - 2re)f_r - (p + r)\sin\theta f_\theta] \quad (27)$$

where $p = a(1 - e^2)$, $h = \sqrt{\mu p}$, $n = \sqrt{\mu/a^3}$, and $r = p/(1 + e\cos\theta)$. Instead of using the mean anomaly, we choose the eccentric anomaly as the sixth orbital element.

$$\frac{\mathrm{d}E}{\mathrm{d}t} = \frac{na}{r} + \frac{1}{nae}\left[f_r(\cos\theta - e) - f_\theta\left(1 + \frac{r}{a}\right)\sin\theta\right] \quad (28)$$

Assuming that the acceleration (f_r and f_θ) level is much smaller than the gravitational acceleration, Eq. (28) can be approximated as

$$\frac{\mathrm{d}E}{\mathrm{d}t} \approx \frac{na}{r} \quad (29)$$

The transformations between eccentric anomaly E and true anomaly θ are given by

$$\sin\theta = \frac{\sin E\sqrt{1 - e^2}}{1 - e\cos E} \quad (30)$$

$$\cos\theta = \frac{\cos E - e}{1 - e\cos E} \quad (31)$$

Therefore, derivatives of the first five classical orbital elements $(a, e, i, \Omega, \omega)$ with respect to eccentric anomaly E can be computed by dividing Gauss' variational equations (22–26) by Eq. (28)

$$\frac{\mathrm{d}a}{\mathrm{d}E} = \frac{2a^3}{\mu}(f_r e\sin E + f_\theta\sqrt{1 - e^2}) \quad (32)$$

$$\frac{\mathrm{d}e}{\mathrm{d}E} = \frac{a^2}{\mu}[f_r(1 - e^2)\sin E + f_\theta(2\cos E - e - e\cos^2 E)\sqrt{1 - e^2}] \quad (33)$$

$$\frac{\mathrm{d}i}{\mathrm{d}E} = \frac{a^2}{\mu}f_n\left(\frac{\cos\omega\cos E - e\cos\omega}{\sqrt{1 - e^2}} - \sin\omega\sin E\right)(1 - e\cos E) \quad (34)$$

$$\frac{\mathrm{d}\Omega}{\mathrm{d}E} = \frac{a^2}{\mu}f_n\left(\frac{\sin\omega\cos E - e\sin\omega}{\sqrt{1 - e^2}} + \cos\omega\sin E\right)\frac{(1 - e\cos E)}{\sin i} \quad (35)$$

$$\frac{\mathrm{d}\omega}{\mathrm{d}E} = -\cos i\frac{\mathrm{d}\Omega}{\mathrm{d}E} - \frac{a^2}{e\mu}[f_r(\cos E - e)\sqrt{1 - e^2} - f_\theta(2 - e^2 - e\cos E)\sin E] \quad (36)$$

Because the thrust is very low, we assume that over an orbital arc the classical orbital elements $(a, e, i, \Omega, \omega)$ and acceleration components (f_{in}, f_n) are constant. The incremental changes in classical orbital elements due to each proposed control law can be obtained by integrating Eqs. (32–36) with respect to eccentric anomaly.

The pitch steering angle α is used to denote the thrust component direction in the orbital plane such that $f_r = f_{\mathrm{in}}\sin\alpha$ and $f_\theta = f_{\mathrm{in}}\cos\alpha$ [see Eqs. (32), (33), and (36)]. For the tangential steering (along the velocity direction), α can be determined by setting $\partial(\mathrm{d}a/\mathrm{d}E)/\partial\alpha = 0$ and $\partial^2(\mathrm{d}a/\mathrm{d}E)/\partial\alpha^2 \le 0$

$$\sin\alpha = \frac{e\sin E}{\sqrt{1 - e^2\cos^2 E}} \quad (37)$$

$$\cos\alpha = \frac{\sqrt{1 - e^2}}{\sqrt{1 - e^2\cos^2 E}} \quad (38)$$

The incremental changes in classical orbital elements using the tangential steering only with respect to eccentric anomaly from E_0 to E_f are obtained [14]

$$\text{delta}\,\mathbf{x}(f_{\mathrm{in}}, 0, [E_0, E_f], \text{“Tangential”}) = \begin{bmatrix} \int_{E_0}^{E_f}\frac{\mathrm{d}a}{\mathrm{d}E}\,\mathrm{d}E = \frac{2a^3}{\mu}f_{\mathrm{in}}\int_{E_0}^{E_f}\sqrt{1 - e^2\cos^2 E}\,\mathrm{d}E \\ \int_{E_0}^{E_f}\frac{\mathrm{d}e}{\mathrm{d}E}\,\mathrm{d}E = \frac{2a^2}{e\mu}(1 - e^2)f_{\mathrm{in}}\left\{\int_{E_0}^{E_f}\sqrt{1 - e^2\cos^2 E}\,\mathrm{d}E - \int_{E_0}^{E_f}\frac{1}{\sqrt{1 - e^2\cos^2 E}}\,\mathrm{d}E \quad + [\ell_n(\sin E + \frac{1}{e}\sqrt{1 - e^2\cos^2 E})]_{E_0}^{E_f}\right\} \\ \int_{E_0}^{E_f}\frac{\mathrm{d}i}{\mathrm{d}E}\,\mathrm{d}E = 0 \\ \int_{E_0}^{E_f}\frac{\mathrm{d}\Omega}{\mathrm{d}E}\,\mathrm{d}E = 0 \\ \int_{E_0}^{E_f}\frac{\mathrm{d}\omega}{\mathrm{d}E}\,\mathrm{d}E = -\frac{2a^2}{e^2\mu}\sqrt{1 - e^2}f_{\mathrm{in}}[\sqrt{1 - e^2\cos^2 E} + \sin^{-1}(e\cos E)]_{E_0}^{E_f} \end{bmatrix} \quad (39)$$

Note the incremental changes in classical orbital elements are denoted by delta$\mathbf{x}$(arg 1, arg 2, [arg 3, arg 4], arg 5) where arg 1 denotes in-plane acceleration amplitude, arg 2 denotes out-of-plane acceleration amplitude, arg 3 and arg 4 denote the starting and ending angles over a revolution for integration, respectively, and arg 5 denotes the type of steering (tangential or inertial or yaw). The same expression will be used for incremental changes in classical orbital elements using the inertial and constant yaw steering. In Eq. (39), we are unable to find the analytic expressions for the terms $\int_{E_0}^{E_f}\sqrt{1 - e^2\cos^2 E}\,\mathrm{d}E$ and $\int_{E_0}^{E_f}\frac{1}{\sqrt{1 - e^2\cos^2 E}}\,\mathrm{d}E$. However, the following approximations for the integrands are used:

$$\sqrt{1 - e^2\cos^2 E} \approx \sqrt{1 - e^2} + (1 - \sqrt{1 - e^2})\sin^2 E \quad (40)$$

$$\sqrt{1 - e^2\cos^2 E} - \frac{1}{\sqrt{1 - e^2\cos^2 E}} = \frac{-e^2\cos^2 E}{\sqrt{1 - e^2\cos^2 E}} \approx \frac{-e^2\cos^2 E}{\sqrt{1 - e^2}c} \quad (41)$$

The corresponding integrals of the approximated integrands are

expressed in Eqs. (42) and (43) [14].

$$\int_{E_0}^{E_f} \sqrt{1-e^2\cos^2 E}\,\mathrm{d}E \approx [\sqrt{1-e^2}E + (1-\sqrt{1-e^2})(0.5E - 0.25\sin 2E)]_{E_0}^{E_f} \tag{42}$$

$$\int_{E_0}^{E_f} \sqrt{1-e^2\cos^2 E}\,\mathrm{d}E - \int_{E_0}^{E_f} \frac{1}{\sqrt{1-e^2\cos^2 E}}\,\mathrm{d}E \approx \frac{-e^2}{\sqrt{1-e^2}c}[0.5E + 0.25\sin 2E]_{E_0}^{E_f} \tag{43}$$

In Eqs. (41) and (43), a constant value c is introduced for the approximation. By choosing $c = 0.8$, the approximations in Eqs. (41) and (43) exhibit satisfactory accuracy, which is shown in [14] by comparing tangential-thrust trajectory propagation results obtained by averaging technique and precise integration. Note that if antitangential steering is used, the incremental changes can be given by $-\mathrm{delta}\mathbf{x}(f_{\mathrm{in}}, 0, [E_0, E_f], \mathrm{Tangential})$.

The inertial steering discussed in this work is defined as $\alpha = \theta$ to increase the eccentricity, and $\alpha = \pi + \theta$ to decrease the eccentricity. Note the inertial steering is always perpendicular to the orbit semimajor axis over each orbital revolution. If the inertial steering ($\alpha = \theta$, no yaw steering) is used over an arc from eccentric anomaly E_0 to E_f, the incremental changes in classical orbital elements can be obtained in a pure analytic form without any need of approximations [see Eq. (44)]. If $\alpha = \pi + \theta$ is employed to decrease the eccentricity, the incremental changes in classical orbital elements can be denoted by $-\mathrm{delta}\mathbf{x}(f_{\mathrm{in}}, 0, [E_0, E_f], \mathrm{Inertial})$. Note again that the inertial steering provide a near-optimal strategy to change the eccentricity.

$$\mathrm{delta}\,\mathbf{x}(f_{\mathrm{in}}, 0, [E_0, E_f], \mathrm{Inertial}) = \begin{bmatrix} \int_{E_0}^{E_f} \frac{\mathrm{d}a}{\mathrm{d}E}\,\mathrm{d}E = \frac{2a^3}{\mu} f_{\mathrm{in}}\sqrt{1-e^2}[\sin E]_{E_0}^{E_f} \\ \int_{E_0}^{E_f} \frac{\mathrm{d}e}{\mathrm{d}E}\,\mathrm{d}E = \frac{a^2}{\mu} f_{\mathrm{in}}\sqrt{1-e^2}[1.5E - 2e\sin E + 0.25\sin 2E]_{E_0}^{E_f} \\ \int_{E_0}^{E_f} \frac{\mathrm{d}i}{\mathrm{d}E}\,\mathrm{d}E = 0 \\ \int_{E_0}^{E_f} \frac{\mathrm{d}\Omega}{\mathrm{d}E}\,\mathrm{d}E = 0 \\ \int_{E_0}^{E_f} \frac{\mathrm{d}\omega}{\mathrm{d}E}\,\mathrm{d}E = -\frac{a^2}{e\mu} f_{\mathrm{in}}[0.25\cos 2E - e\cos E]_{E_0}^{E_f} \end{bmatrix} \tag{44}$$

The constant yaw steering is employed to change the orbital plane, which allows us to find the analytic incremental changes in classical orbital elements over an arc from eccentric anomaly E_0 to E_f, which is shown in Eq. (45).

$$\begin{aligned} &\mathrm{delta}\,\mathbf{x}(f_{\mathrm{in}}, 0, [E_0, E_f], \mathrm{Yaw}) \\ &= \begin{bmatrix} \int_{E_0}^{E_f} \frac{\mathrm{d}a}{\mathrm{d}E}\,\mathrm{d}E = 0 & \\ \int_{E_0}^{E_f} \frac{\mathrm{d}e}{\mathrm{d}E}\,\mathrm{d}E = 0 & \\ \int_{E_0}^{E_f} \frac{\mathrm{d}i}{\mathrm{d}E}\,\mathrm{d}E = \frac{a^2}{\mu} f_n[& \frac{(1+e^2)\cos\omega\sin E - 1.5eE\cos\omega - 0.25e\cos\omega\sin 2E}{\sqrt{1-e^2}} + \sin\omega\cos E - 0.25e\sin\omega\cos 2E]_{E_0}^{E_f} \\ \int_{E_0}^{E_f} \frac{\mathrm{d}\Omega}{\mathrm{d}E}\,\mathrm{d}E = \frac{a^2}{\mu\sin i} f_n[& \frac{(1+e^2)\sin\omega\sin E - 1.5eE\sin\omega - 0.25e\sin\omega\sin 2E}{\sqrt{1-e^2}} - \cos\omega\cos E + 0.25e\cos\omega\cos 2E]_{E_0}^{E_f} \\ \int_{E_0}^{E_f} \frac{\mathrm{d}\omega}{\mathrm{d}E}\,\mathrm{d}E = -\cos i \int_{E_0}^{E_f} \frac{\mathrm{d}\Omega}{\mathrm{d}E}\,\mathrm{d}E & \end{bmatrix} \end{aligned} \tag{45}$$

Therefore, the total incremental change in classical orbital elements for an orbital revolution is (using the case in Fig. 1 as an example)

$$\begin{aligned} \int_{\bar{E}_{\mathrm{ex}}}^{\bar{E}_{\mathrm{en}}} \frac{\mathrm{d}\mathbf{x}}{\mathrm{d}E}\,\mathrm{d}E &= \mathrm{delta}\mathbf{x}(0, f, [\bar{E}_{\mathrm{ex}}, \bar{s}_1], \mathrm{Yaw}) + \mathrm{delta}\mathbf{x}(\sqrt{f^2 - f_n^2}, 0, [\bar{s}_1, \bar{y}_2], \mathrm{Tangential}) + \mathrm{delta}\mathbf{x}(0, f_n, [\bar{s}_1, \bar{y}_2], \mathrm{Yaw}) \\ &+ \mathrm{delta}\mathbf{x}(f, 0, [\bar{y}_2, \bar{s}_2], \mathrm{Tangential}) + \mathrm{delta}\mathbf{x}(0, f, [\bar{y}_3, \bar{e}_1], \mathrm{Yaw}) + \mathrm{delta}\mathbf{x}(\sqrt{f^2 - f_n^2}, 0, [\bar{e}_1, \bar{y}_4], \mathrm{Inertial}) + \mathrm{delta}\mathbf{x}(0, f_n, [\bar{e}_1, \bar{y}_4], \mathrm{Yaw}) \\ &+ \mathrm{delta}\mathbf{x}(f, 0, [\bar{y}_4, \bar{e}_2], \mathrm{Inertial}) \end{aligned} \tag{46}$$

Note there is no thrust over the orbital arc from s_2 to y_3, and from e_2 to E_{en}. Moreover, the shadow entrance/exit angles E_{en} and E_{ex} are computed for each orbital revolution in terms of the corresponding calendar date. The overbar "‾" in Eq. (46) denotes the values in eccentric anomaly, which are converted from corresponding true anomalies using the following transformations:

$$\sin E = \frac{\sin\theta\sqrt{1-e^2}}{1 + e\cos\theta} \tag{47}$$

$$\cos E = \frac{e + \cos\theta}{1 + e\cos\theta} \tag{48}$$

In this example, computing the incremental changes in classical orbital elements over a revolution requires several integration steps. The integral limits of each integration step are determined by the sequence order of s_1, s_2, e_1, e_2 y_1, y_2, y_3, and y_4 along the orbital arc from $\bar{E}_{\mathrm{ex}}$ to $\bar{E}_{\mathrm{en}}$. A different sequence order might result in a different expression of Eq. (46). That is to say, we need to find the sequence order of $s_1, s_2, e_1, e_2\, y_1, y_2$, y_3, and y_4 to compute $\int_{\bar{E}_{\mathrm{ex}}}^{\bar{E}_{\mathrm{en}}} \frac{\mathrm{d}\mathbf{x}}{\mathrm{d}E}\,\mathrm{d}E$ in Eq. (46).

In addition to incremental changes in classical orbital elements, the averaging mass loss from $\bar{E}_{\mathrm{ex}}$ to $\bar{E}_{\mathrm{en}}$ is computed as (using the case in Fig. 1 as an example)

$$\Delta m = -\frac{f}{gI_{\mathrm{sp}}} \cdot \frac{1}{n}[(\bar{E}_{\mathrm{ex}} - e\sin\bar{E}_{\mathrm{ex}} - \bar{s}_2 + e\sin\bar{s}_2) + (\bar{y}_3 - e\sin\bar{y}_3 - \bar{e}_2 + e\sin\bar{e}_2)] \tag{49}$$

where $f = 2\eta P/(gI_{\mathrm{sp}})$. Equation (49) indicates that there is no mass loss from s_2 to y_3, and from e_2 to E_{en} because there is no thrust in the corresponding orbital arcs. Additionally, the period of each orbital revolution is

$$\Delta t = \frac{2\pi}{n} \tag{50}$$

Furthermore, the averaging changes in classical orbital elements due to J_2 perturbations are as follows:

$$\frac{\mathrm{d}\bar{a}}{\mathrm{d}t} = \frac{\mathrm{d}\bar{e}}{\mathrm{d}t} = \frac{\mathrm{d}\bar{i}}{\mathrm{d}t} = 0 \tag{51}$$

$$\frac{\mathrm{d}\bar{\Omega}}{\mathrm{d}t} = -\frac{3}{2} J_2 \frac{r_e^2}{a^2(1-e^2)^2} n \cos i \tag{52}$$

$$\frac{\mathrm{d}\bar{\omega}}{\mathrm{d}t} = \frac{3}{4} J_2 \frac{r_e^2}{a^2(1-e^2)^2} n(5\cos^2 i - 1) \tag{53}$$

Therefore, the total incremental changes in classical orbital elements including low-thrust acceleration, J_2 perturbations, and the Earth's shadow for each orbital revolution is computed as

$$\Delta \mathbf{x} = \int_{E_{\mathrm{ex}}}^{E_{\mathrm{en}}} \frac{\mathrm{d}\mathbf{x}}{\mathrm{d}E}\, \mathrm{d}E + \frac{\mathrm{d}\bar{\mathbf{x}}}{\mathrm{d}t} \frac{2\pi}{n} \tag{54}$$

With $\mathbf{y} = [\mathbf{x}\ t\ m]$ and $\Delta \mathbf{y} = [\Delta \mathbf{x}\ \Delta t\ \Delta m]$, the elements in the $(i+1)$ th revolution are computed only in terms of the elements in the (i)th revolution.

$$\mathbf{y}_{i+1} = \mathbf{y}_i + \Delta \mathbf{y}_i \tag{55}$$

Equation (54) is computed for each revolution within which the orbital elements $(a, e, i, \Omega, \omega)$ and thrust accelerations are constant (thus the locations of perigee and apogee do not change). Therefore, within each orbital revolution the inertial steering perpendicular to the semimajor axis is truly inertial, and the control laws termed by "perigee-" or "apogee-centered steering" and derived from Eq. (12) are truly correctly defined. Furthermore, the Earth's shadow remains the same as well within each orbital revolution but recomputed for the next revolution in terms of the corresponding calendar date. In fact, the orbital elements, mass, and time are propagated in terms of Eq. (55) at the interval of an orbital revolution or an orbital period.

The final states are obtained by interpolating the classical orbital elements during the last revolution in terms of the final time. For example, if the final time t_f is specified, a linear interpolation in Eq. (56) is used to determine $\mathbf{y}_f$ as $t_i < t_f < t_{i+1}$ using $\mathbf{y}_i$ and $\mathbf{y}_{i+1}$.

$$\mathbf{y}_f = \mathbf{y}_i + \frac{t_f - t_i}{t_{i+1} - t_i}(\mathbf{y}_{i+1} - \mathbf{y}_i) \tag{56}$$

The proposed analytic orbital averaging technique gives five classical orbital elements and the number of trajectory revolutions at the prespecified terminal time. Note that the technique is only valid when the orbit is elliptic (i.e., eccentricity is less than 1). Trajectory propagation using the analytic orbital averaging technique significantly reduces the simulation time. Even though we compute the incremental changes in classical orbital elements for each revolution, final states can be obtained within a second for a trajectory with a thousand revolutions on current PC computers. Based on the fast trajectory propagation, trajectory optimization using nonlinear programming is developed in the following section.

Trajectory Optimization

As described previously, the parameters related to the control laws are w_s, w_e, w_A, and w_Y for each orbital revolution. To optimize these parameters for the entire transfer trajectory, a finite number of equally spaced nodes along the time axis, denoted by $G_{w_s}(t_i)$, $G_{w_e}(t_i)$, $G_{w_A}(t_i)$, and $G_{w_Y}(t_i)$, are used to represent the time histories of w_s, w_e, w_A, and w_Y. The optimal control problem is then converted to a parameter optimization problem that is in turn solved by nonlinear programming, and sequential quadratic programming (SQP) [15] is employed in this work. Therefore, the SQP design variables are $G_{w_s}(t_i)$, $G_{w_e}(t_i)$, $G_{w_A}(t_i)$, $G_{w_Y}(t_i)$, and the transfer time t_f. For each orbital revolution, w_s, w_e, w_A, and w_Y are obtained using the linear interpolation through the nodes $G_{w_s}(t_i)$, $G_{w_e}(t_i)$, $G_{w_A}(t_i)$, and $G_{w_Y}(t_i)$ in terms of the time t_i. The desired performance (e.g., minimum t_f or maximum mass at t_f) is directly optimized by the performance index function of the SQP subroutine. The upper and lower bounds of $G_{w_s}(t_i)$, $G_{w_e}(t_i)$, $G_{w_A}(t_i)$, and $G_{w_Y}(t_i)$ are set through the uncertainty interval of SQP design variables. The other constraint set through an SQP inequality constraint is

$$|G_{w_s}(t_i)| + |G_{w_e}(t_i)| \le 1 \tag{57}$$

Equation (57) indicates that no overlap exists between the orbital arc from s_1 to s_2 and the arc from e_1 to e_2.

If we let $s_1 = e_2$ and $s_2 = e_1$, we obtain $|G_{w_s}(t_i)| + |G_{w_e}(t_i)| = 1$, which means the thrust is always continuous out of the Earth's shadow. If we set SQP performance as the minimum t_f, the formulation of minimum-time transfer problems can be simplified with $s_1 = e_2$ and $s_2 = e_1$. In this case, either $G_{w_s}(t_i)$ or $G_{w_e}(t_i)$ can be removed from the SQP variables to reduce the dimension of the proposed SQP problem, and thus the inequality constraint Eq. (57) is not necessary [16]. For example, we can get $G_{w_s}(t_i) = 1 - |G_{w_e}(t_i)|$ if $G_{w_e}(t_i)$ is to be optimized. Furthermore, we can set $G_{w_s}(t_i) > 0$ for orbital raising transfers, and $G_{w_s}(t_i) < 0$ for orbital descending transfers.

The nodes $G_{w_s}(t_i) \in [-1 \quad 1]$, $G_{w_e}(t_i) \in [-1 \quad 1]$, $G_{w_A}(t_i) \in [-1 \quad 1]$, and $G_{w_Y}(t_i) \in [0 \quad 1]$, which are all bounded, have evident physical meanings. For $G_{w_s}(t_i)$, $G_{w_e}(t_i)$, and $G_{w_A}(t_i)$, plus and minus signs mean increasing and reducing the corresponding orbital element (a, e, i), respectively, and the larger the absolute values are the more the orbital elements change. In addition, $G_{w_Y}(t_i) = 0$ means that the yaw steering is always applied, and $G_{w_Y}(t_i) = 1$ means no yaw steering. We can run nominal trajectories by adjusting the values of these nodes along the time history as well as t_f with trial and error to find candidate transfers with terminal orbital elements close to the target orbit's constraints. The candidate transfers are then deemed as good initial guesses for optimization.

Guidance Scheme Design

As we know, the proposed approach is an approximate one for computing near-optimal Earth-orbit transfer problems, and the control strategy is simple and only a small number of parameters are used to determine the control laws. Based on the control laws shown in Fig. 1, the guidance control scheme can be proposed as follows at the time point t where $0 \le t \le t_f$.

Minimum-Fuel Guidance Scheme

1) Determine f_n and f_{in} if the spacecraft is not in the Earth's shadow

$$\left[\frac{\mathrm{d}i}{\mathrm{d}t}\right]_{\max} = \max\left(\left|\frac{\cos(\omega(t) + \theta_1^m)}{1 + e\cos(\theta_1^m)}\right|, \left|\frac{\cos(\omega(t) + \theta_2^m)}{1 + e\cos(\theta_2^m)}\right|\right)$$

where

$$\theta_1^m = \sin^{-1}(-e\sin\omega(t)) - \omega(t)$$

$$\theta_2^m = \pi - \sin^{-1}(-e\sin\omega(t)) - \omega(t)$$

$$f_n = \begin{cases} \neq 0 & \text{if } \left|\frac{\cos(\omega(t)+\theta(t))}{1+e\cos(\theta(t))}\right| \ge w_Y(t)\left[\frac{\mathrm{d}i}{\mathrm{d}t}\right]_{\max} \\ =0 & \text{otherwise} \end{cases}$$

$$f_{\text{in}} = \begin{cases} \neq 0 & \text{if } \cos(\theta(t)) \le \cos(\pi - |w_e(t)|\pi) \quad \text{or} \quad \cos(\theta(t)) \ge \cos(-|w_s(t)|\pi) \\ =0 & \text{otherwise} \end{cases}$$

Cases:

$$\text{if } f_n \neq 0 \quad \text{and} \quad f_{\text{in}} \neq 0\text{: } f_n = f \cdot w_A(t) \cdot \text{sign}[\cos(\omega(t) + \theta(t))] \quad \text{and} \quad f_{\text{in}} = f\sqrt{1 - w_A(t)^2}$$

$$\text{if } f_n \neq 0 \quad \text{and} \quad f_{\text{in}} = 0\text{: } f_n = f \cdot \text{sign}(w_A(t)) \cdot \text{sign}[\cos(\omega(t) + \theta(t))] \quad \text{and} \quad f_{\text{in}} = 0$$

$$\text{if } f_n = 0 \quad \text{and} \quad f_{\text{in}} \neq 0\text{: } f_n = 0 \quad \text{and} \quad f_{\text{in}} = f$$

$$\text{if } f_n = 0 \quad \text{and} \quad f_{\text{in}} = 0\text{: } f_n = 0 \quad \text{and} \quad f_{\text{in}} = 0$$

2) Determine the pitch angle α, f_r, and f_θ if $f_{\text{in}} \neq 0$

$$\alpha = \begin{cases} \begin{cases} \theta & \text{if } w_e(t) > 0 \\ \pi + \theta & \text{if } w_e(t) < 0 \end{cases} & \text{if } \cos(\theta(t)) \le \cos(\pi - |w_e(t)|\pi) \\ \begin{cases} \gamma & \text{if } w_s(t) > 0 \\ -\gamma & \text{if } w_s(t) < 0 \end{cases} & \text{if } \cos(\theta(t)) \ge \cos(-|w_s(t)|\pi) \end{cases}$$

$$f_r = f_{\text{in}} \sin\alpha, \qquad f_\theta = f_{\text{in}} \cos\alpha$$

Note if the spacecraft is in the Earth's shadow at time t, the thrust is set to zero. Parameters $w_s(t)$, $w_e(t)$, $w_A(t)$, and $w_Y(t)$ are linearly interpolated using the optimal nodes of $G_{w_s}(t_i)$, $G_{w_e}(t_i)$, $G_{w_A}(t_i)$, and $G_{w_Y}(t_i)$ obtained by trajectory optimization results.

Minimum-Time Guidance Scheme

If the minimum-time transfer is desired, we can set $|G_{w_s}(t_i)| + |G_{w_e}(t_i)| = 1$, which implies that the thrust is always continuous out of the Earth's shadow. The guidance scheme can be written in a simpler form:

1) Determine f_n and f_{in}

$$\left[\frac{\mathrm{d}i}{\mathrm{d}t}\right]_{\max} = \max\left(\left|\frac{\cos(\omega(t) + \theta_1^m)}{1 + e\cos(\theta_1^m)}\right|, \left|\frac{\cos(\omega(t) + \theta_2^m)}{1 + e\cos(\theta_2^m)}\right|\right)$$

where

$$\theta_1^m = \sin^{-1}(-e\sin\omega(t)) - \omega(t)$$

$$\theta_2^m = \pi - \sin^{-1}(-e\sin\omega(t)) - \omega(t)$$

$$f_n = \begin{cases} =f \cdot w_A(t) \cdot \text{sign}[\cos\omega(t) + \theta(t))] & \text{if } \left|\frac{\cos(\omega(t)+\theta(t))}{1+e\cos(\theta(t))}\right| \ge w_Y(t)\left[\frac{\mathrm{d}i}{\mathrm{d}t}\right]_{\max} \\ =0 & \text{otherwise} \end{cases}$$

$$f_{\text{in}} = \sqrt{f^2 - f_n^2}$$

2) Determine the pitch angle α, f_r and f_θ

$$\alpha = \begin{cases} \begin{cases} \theta & \text{if } w_e(t) > 0 \\ \pi + \theta & \text{if } w_e(t) < 0 \end{cases} & \text{if } \cos\theta(t) \le \cos(\pi - |w_e(t)|\pi) \\ \begin{cases} \gamma & \text{if } w_s(t) > 0 \\ -\gamma & \text{if } w_s(t) < 0 \end{cases} & \text{otherwise} \end{cases}$$

$$f_r = f_{\text{in}} \sin\alpha, \qquad f_\theta = f_{\text{in}} \cos\alpha$$

Likewise, the thrust is set to zero if the spacecraft is in the Earth's shadow at time t, and parameters $w_s(t)$, $w_e(t)$, $w_A(t)$, and $w_Y(t)$ are linearly interpolated using the optimal nodes of $G_{w_s}(t_i)$, $G_{w_e}(t_i)$, $G_{w_A}(t_i)$, and $G_{w_Y}(t_i)$ obtained by trajectory optimization results. The minimum-time guidance scheme is a special case of the minimum-fuel guidance scheme.

In this paper, the proposed guidance scheme relies only on a small number of parameters $G_{w_s}(t_i)$, $G_{w_e}(t_i)$, $G_{w_A}(t_i)$, $G_{w_Y}(t_i)$, and t_f. With these parameters and orbital element information from the orbit determination system, the control laws can be constructed at time t. The parameters $G_{w_s}(t_i)$, $G_{w_e}(t_i)$, $G_{w_A}(t_i)$, $G_{w_Y}(t_i)$, and t_f can be recalculated on the ground and uplinked to the spacecraft every few days. This kind of trajectory recalculating scheme requires a small amount of information to be uplinked so that both onboard storage and communication costs are minimized.

Numerical Examples

Minimum-Time Transfers

Three example transfers from a low Earth orbit (LEO) to a geostationary equatorial orbit (GEO), from geostationary transfer orbit (GTO) to GEO, and from LEO to a global-positioning-system (GPS) orbit are solved. The parameters of different orbits are summarized in Table 1, and the spacecraft parameters for the three transfer cases are defined in Table 2. Optimal transfers for the first two cases have been obtained in [6] using a direct method (DM) and SEPSPOT.

For all cases, 10 nodes each are used for $G_{w_s}(t_i)$, $G_{w_e}(t_i)$, $G_{w_A}(t_i)$, and $G_{w_Y}(t_i)$ and the nodal values are equally spaced during the transfer time history. After including t_f as an optimization variable, there are a total of 41 SQP design variables for the NLP problem. All cases involve Earth J_2 and shadow effects. The initial dates for all cases are set at 1 January 2000 to correspond to [6]. The transfer time t_f is directly minimized by SQP.

A comparison of the solutions obtained by the proposed approach, DM, and SEPSPOT is presented in Table 3 (for cases 1 and 2) [6]. The transfer times (and propellant masses) for the near-optimal solutions are slightly greater (about 5%) than the transfer times (and propellant masses) computed by DM and SEPSPOT. As mentioned in the Introduction, the computational burden is greatly reduced by using the orbital averaging compared with direct methods. The analytic incremental changes in classical orbital elements are addressed to distinguish the orbital averaging used in this paper from the one in other articles. For example, DM in [6] obtains the incremental changes in classical orbital elements using a numerical integration method, which requires a finite number of integration steps and more computational time than the analytic approach in this paper. The analytic orbital averaging propagates trajectories at the interval of an orbital revolution while DM in [6] propagates trajectories at the two-day interval. Besides the method to obtain incremental changes of orbital elements and trajectory propagation step size, the overall computational cost also depends on the number of nodes for $G_{w_s}(t_i)$, $G_{w_e}(t_i)$, $G_{w_A}(t_i)$, and $G_{w_Y}(t_i)$, which parameterize the time histories of control profiles.

Table 1 Orbit parameters

Orbits	$a(R_e)$	e	i, deg	Ω, deg	ω, deg
LEO	1.086	10^{-4}	28.5	0	0
GTO	3.820	0.731	27	99	0
GEO	6.6107	10^{-4}	10^{-4}	——	——
GPS	4.0764	10^{-4}	60	——	——

Table 2 Spacecraft parameters and transfer cases

Case	P, kW	I_{sp}, s	η	m_0, kg	Initial thrust-to-weight ratio	Transfer type
1	10	3300	0.65	1200	3.41×10^{-5}	LEO–GEO
2	5	3300	0.65	450	4.55×10^{-5}	GTO–GEO
3	10	3300	0.65	1200	3.41×10^{-5}	LEO–GPS

Table 3 Optimal solutions obtained by three methods (in year 2000)

Case	t_f, days	m_f, kg	t_f, (DM) [6], days	t_f, (SEPSPOT) [6], days
1	202.9	1002.48	200.3	198.9
2	70.2	413.55	67.0	66.6
3	205.7	1000.68	——	——

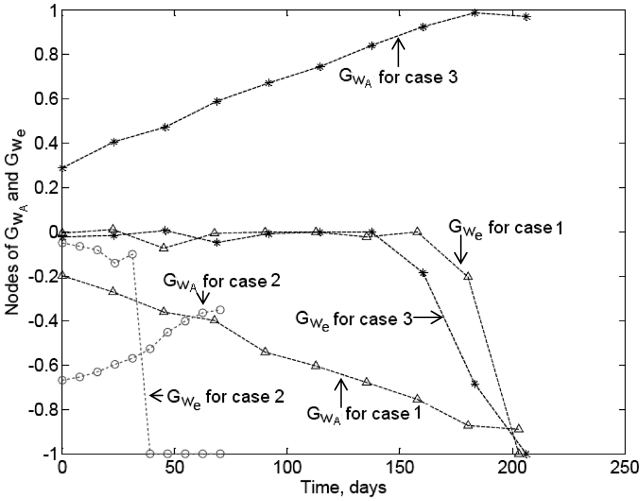

Fig. 3 Optimal values of nodes $G_{w_A}(t_i)$ and $G_{w_e}(t_i)$.

For minimum-time transfers, strategies to reduce the dimension of the NLP problem are 1) removing nodes of $G_{w_s}(t_i)$ by using $G_{w_s}(t_i) = 1 - |G_{w_e}(t_i)|$ [$G_{w_s}(t_i) > 0$ for orbital raising]. 2) $G_{w_Y}(t_i)$ is represented by a single constant (not 10 nodes). It is found that almost the same results shown in Table 3 are obtained (reducing NLP dimension does not obtain a worse performance). In fact, the constraint $|G_{w_s}(t_i)| + |G_{w_e}(t_i)| = 1$ is reached if nodes of both $G_{w_s}(t_i)$ and $G_{w_e}(t_i)$ are optimized. If $G_{w_Y}(t_i)$ is expressed by a single constant, SQP automatically adjusts amplitudes of the nodes $G_{w_A}(t_i)$. With the above strategies, the total number of design variables is reduced to 22, and the constrained Eq. (57) is not necessary. Figure 3 presents the optimal values for nodes $G_{w_A}(t_i)$ and $G_{w_e}(t_i)$ for all three cases with employing strategies to reduce the dimension. Note that for the LEO–GEO case (case 1), the optimal values of $G_{w_e}(t_i)$ are nearly zero for the majority of the transfer. Therefore, tangential steering is used for the majority of the transfer, and inertial steering is only employed at the end of the transfer to remove residual eccentricity. For the GTO–GEO case (case 2), inertial steering is the sole in-plane steering law at the end of the transfer since $G_{w_e}(t_i) = -1$ for nearly the second half of the transfer. For the LEO–GPS case (case 3), the in-plane steering profile is similar to case 1, but the yaw steering component is relatively large to increase inclination at a lower altitude than the LEO–GEO transfer. The optimal values of w_Y are 0.2628, 0.2260, and 0.2139 for cases 1, 2, and 3, respectively. The smaller the value of w_Y, the longer the orbital arc on which the yaw steering is applied.

Fixed-Time, Minimum-Fuel Transfers

Unlike the minimum-time transfers, the fixed-time, minimum-fuel transfer trajectories might include the coast arcs between the arcs using in-plane tangential and inertial steering accelerations, which may result in discontinuous thrusting out of the Earth's shadow. Therefore, the inequality equation $|G_{w_s}(t_i)| + |G_{w_e}(t_i)| \leq 1$ is set through the SQP routine. The transfer times t_f are fixed at different values, and the final spacecraft masses are maximized by SQP. Ten nodes each for $G_{w_s}(t_i)$, $G_{w_e}(t_i)$, $G_{w_A}(t_i)$, and $G_{w_Y}(t_i)$ are used, and there is a total of 40 SQP design variables. The three transfer cases in Table 2 are considered, and the initial dates for all cases are set for

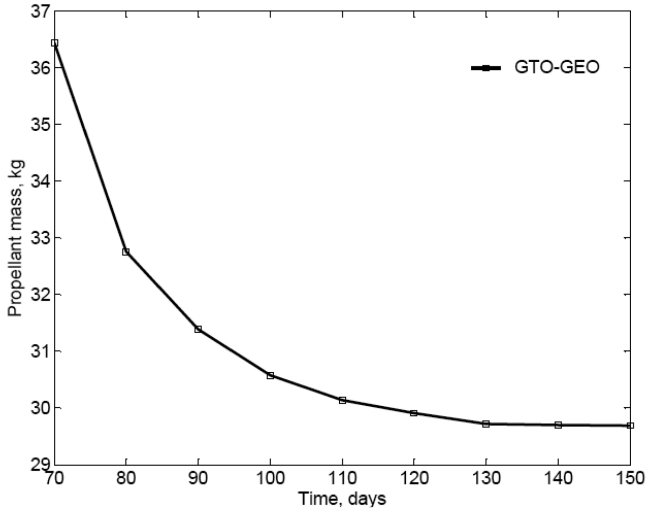

Fig. 4 Propellant mass vs transfer time (GTO–GEO).

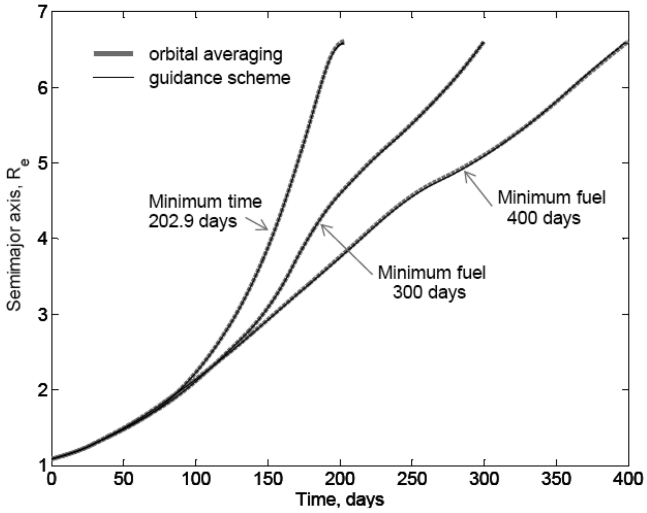

Fig. 6 Time histories of the semimajor axis for LEO–GEO transfers.

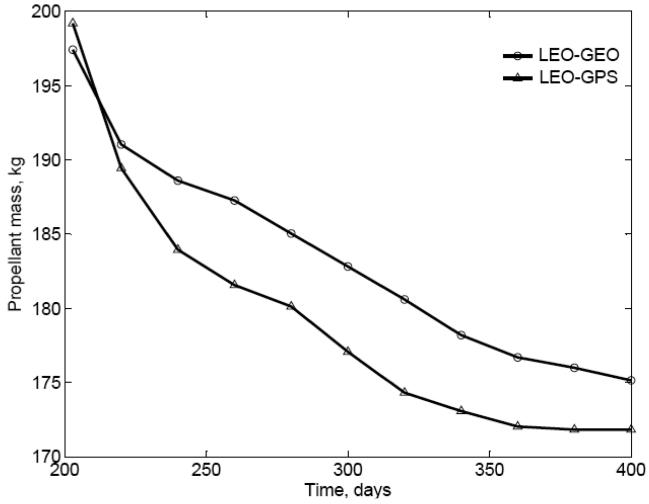

Fig. 5 Propellant mass vs transfer time (LEO–GEO and LEO–GPS).

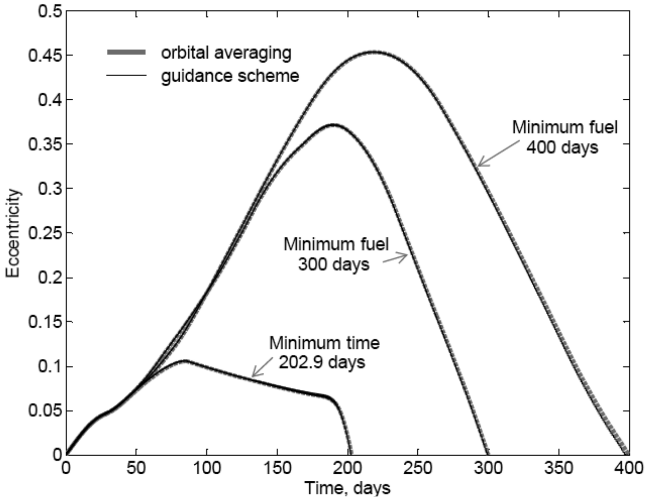

Fig. 7 Time histories of eccentricity for LEO–GEO transfers.

1 January 2008. A series of minimum-fuel solutions for different transfer times are obtained, and the propellant masses and transfer times for all three cases are presented in Figs. 4 and 5 where it is indicated that the fuel consumptions decrease with the increasing of the transfer times. However, the propellant masses decreasing rates become smaller as the transfer times become longer. The almost doubled transfer times save about 12.4, 18.4, and 13.9% of propellant masses for LEO–GEO, GTO–GEO, and LEO–GPS transfers, respectively.

The control laws are parameterized by nodes $G_{w_s}(t_i)$, $G_{w_e}(t_i)$, $G_{w_A}(t_i)$, and $G_{w_Y}(t_i)$, which are directly optimized by the SQP routine. It should be noted that the SQP routine only locates local optimal NLP solutions. Thus, all converged solutions (optimized nodes) obtained are only deemed as local optima. However, the proposed approach demonstrated a novel means, instead of using the optimal control theory, to solve a wide range of very low-thrust transfer problems including Earth oblateness and shadow effects.

Onboard Guidance Schemes

The guidance schemes described in the previous section are used to propagate the spacecraft from the initial orbits (LEO and GTO) to the final orbits (GEO and GPS) with initial dates of 1 January 2008. Parameters $w_s(t)$, $w_e(t)$, $w_A(t)$, and $w_Y(t)$ are linearly interpolated through the nodes of $G_{w_s}(t_i)$, $G_{w_e}(t_i)$, $G_{w_A}(t_i)$, and $G_{w_Y}(t_i)$ that are obtained by NLP optimization for minimum-time and minimum-fuel transfers in the year 2008. A precise integration is used to simulate the orbit transfers in terms of the proposed guidance schemes. The variable step-size fourth-order Runge–Kutta method is used to integrate trajectories with the local and absolute errors set to 10^{-10} to maintain sufficient accuracy. Propellant masses obtained by the orbital averaging and the guidance scheme are compared in Table 4 for all three cases. The errors of propellant mass obtained by the orbital averaging and the guidance scheme are less than 1%. The time histories of semimajor axis, eccentricity, and inclination obtained by precise integration (guidance scheme) for cases 1, 2, and 3 are

Table 4 Propellant masses (kg) vs transfer times (days) using orbital averaging and guidance scheme

	Case 1			Case 2			Case 3		
Times, days	202.9[a]	300	400	70.2[a]	100	150	205.7[a]	300	400
Orbital averaging, mass, kg	197.52	182.82	175.15	36.45	30.58	29.75	199.32	177.07	171.82
Guidance scheme, mass, kg	197.45	183.06	176.92	36.42	30.52	29.69	199.20	177.56	173.04

[a]Transfer times for minimum-time solutions.

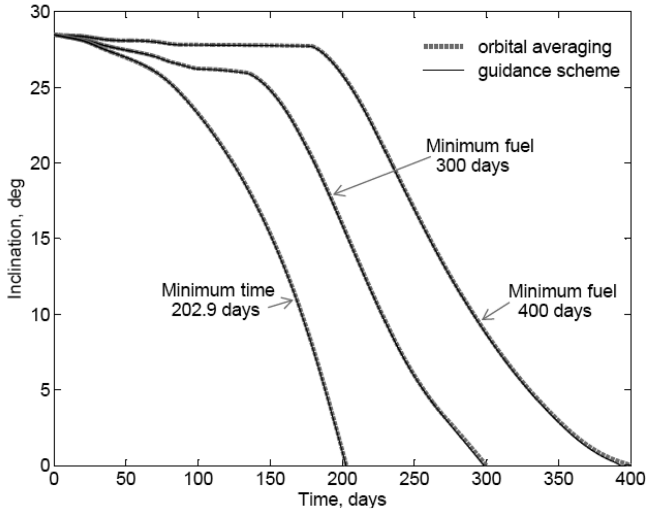

Fig. 8 Time histories of inclination for LEO–GEO transfers.

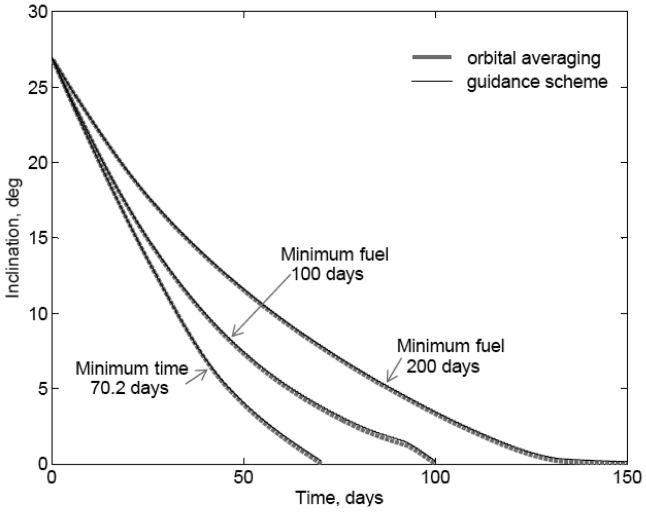

Fig. 11 Time histories of inclination for GTO–GEO transfers.

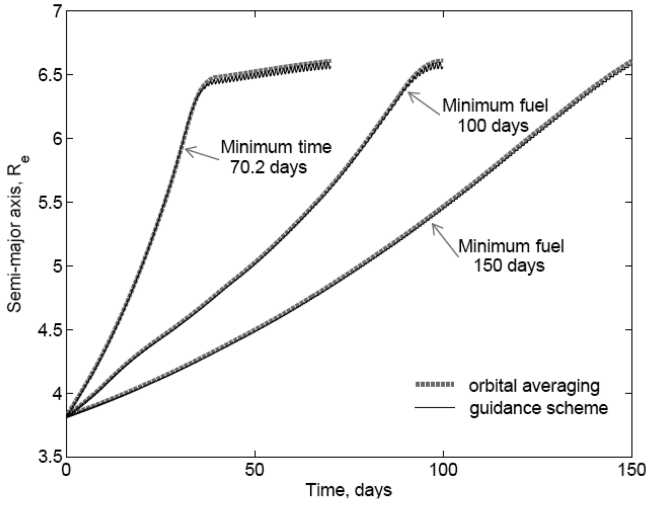

Fig. 9 Time histories of semimajor axis for GTO–GEO transfers.

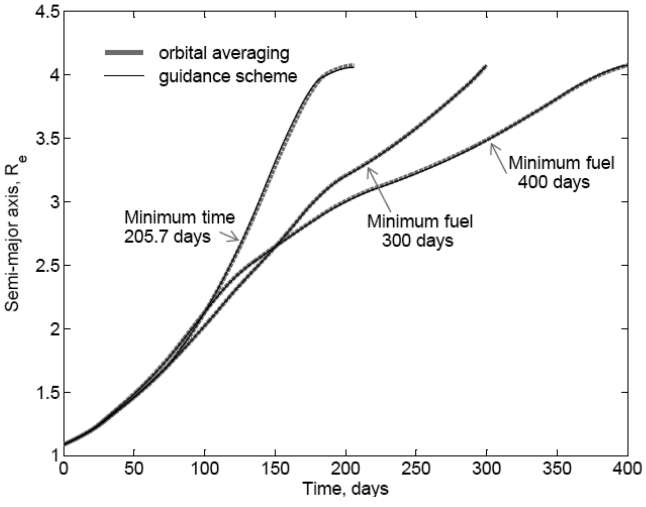

Fig. 12 Time histories of semimajor axis for LEO–GPS transfers.

presented in Figs. 6–8, Figs. 9–11, and Figs. 12–14, respectively. The time histories of mean orbital elements obtained by the orbital averaging are also plotted in the corresponding figures. We can see that the orbital averaging solutions match the full integration solutions very well. The terminal errors are small enough to correct using terminal guidance laws or station keeping maneuvers.

Conclusion

A novel direct optimization approach for obtaining near-optimal very low-thrust Earth orbit in the presence of Earth J_2 and shadow effects has been developed. Both minimum-time and minimum-fuel trajectories involving a coasting mechanism are modeled and solved

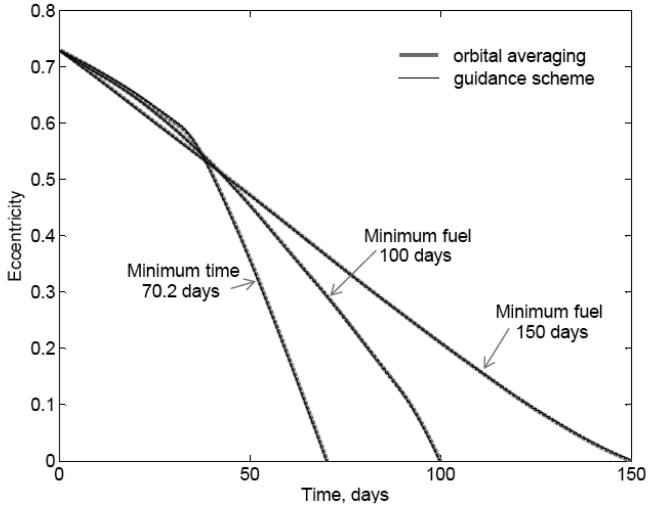

Fig. 10 Time histories of eccentricity for GTO–GEO transfers.

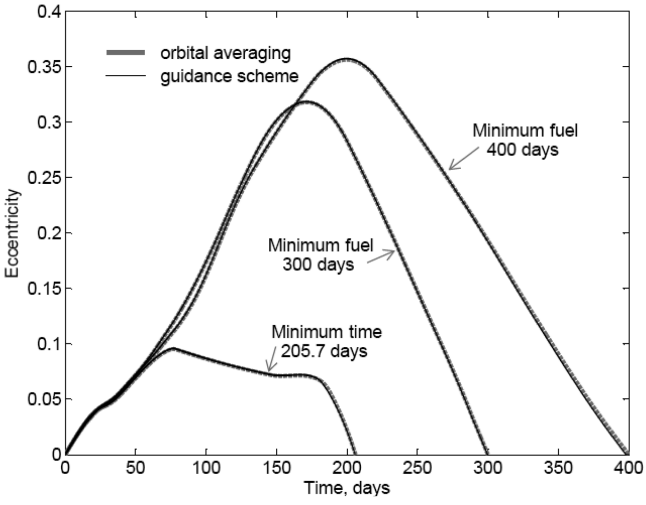

Fig. 13 Time histories of eccentricity for LEO–GPS transfers.

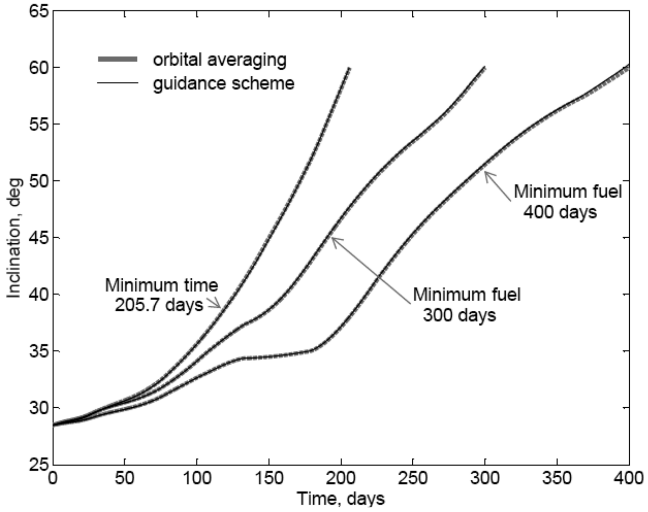

Fig. 14 Time histories of inclination for LEO–GPS transfers.

by parameter optimization formulations. Three typical control laws are employed within each orbital revolution to transfer the spacecraft to the desired orbits. An analytic orbital averaging technique is employed to significantly reduce the computation load for propagating the long-duration, many-revolution trajectories. The parameters to be optimized are bounded and physically intuitive such that good initial guesses can be obtained without much effort. Based on the control strategy and a small number of optimal parameters, onboard guidance schemes are developed to guide the spacecraft to desired orbits. The precise numerical integration is used to simulate the transfer trajectories following the proposed guidance schemes. The results obtained by orbital averaging and guidance scheme match very well between each other. This novel optimization approach would be a useful tool for the preliminary design to determine mission performance, and an onboard guidance scheme could be implemented based on this work.

References

[1] Rayman, M. D., and Williams, S. N., "Design of the First Interplanetary Solar Electric Propulsion Mission," *Journal of Spacecraft and Rockets*, Vol. 39, No. 4, 2002, pp. 589–595.

[2] Koppel, C. R., Marchandise, F., Estublier, D., and Jolivet, L., "The SMART-1 Electric Propulsion Subsystem in Flight Experience," AIAA Paper 2004-3435, 2004.

[3] Sackett, L. L., Malchow, H. L., and Edelbaum, T. N., "Solar Electric Geocentric Transfer with Attitude Constraints: Analysis," NASA CR-134927, Aug. 1975.

[4] Betts, J. T., "Very Low-Thrust Trajectory Optimization Using a Direct SQP Method," *Journal of Computational and Applied Mathematics*, Vol. 120, No. 1, 2000, pp. 27–40.

[5] Scheel, W. A., and Conway, B. A., "Optimization of Very-Low-Thrust, Many-Revolution Spacecraft Trajectories," *Journal of Guidance, Control, and Dynamics*, Vol. 17, No. 6, 1994, pp. 1185–1192.

[6] Kluever, C. A., and Oleson, S. R., "Direct Approach for Computing Near-Optimal Low-Thrust Earth-Orbit Transfers," *Journal of Spacecraft and Rockets*, Vol. 35, No. 4, 1998, pp. 509–515.

[7] Ferrier, C., and Epenoy, R., "Optimal Control for Engines with Electro-Ionic Propulsion Under Constraint of Eclipse," *Acta Astronautica*, Vol. 48, No. 4, 2001, pp. 181–192.

[8] Haberkorn, T., Martinon, P., and Gergaud, J., "Low Thrust Minimum-Fuel Orbital Transfer: A Homotopic Approach," *Journal of Guidance, Control, and Dynamics*, Vol. 27, No. 6, 2004, pp. 1046–1060.

[9] Cailliau, J. B., Gergaud, J., and Noailles, J., "3D Geosynchrotrons Transfer of a Satellite: Continuation on the Thrust," *Journal of Optimization Theory and Applications*, Vol. 118, No. 3, 2003, pp. 541–656.

[10] Spitzer, A., "Near Optimal Transfer Orbit Trajectory Using Electric Propulsion," *Advances in the Astronautical Sciences*, American Astronautical Society, San Diego, CA, Vol. 89, 1995, pp. 1031–1044.

[11] Neta, B., and Vallado, D., "On Satellite Umbra/Penumbra Entry and Exit Positions," *Journal of the Astronautical Sciences*, Vol. 46, No. 1, 1998, pp. 91–104.

[12] Falck, R., and Gefert, L., "A Method of Efficient Inclination Changes for Low-Thrust Spacecraft," AIAA Paper 2002-4895, 2002.

[13] Battin, R. H., *An Introduction to the Mathematics and Methods of Astrodynamics*, AIAA Education Serials, AIAA, Washington, D.C., 1987, pp. 488–489.

[14] Gao, Y., and Kluever, C. A., "Analytic Orbital Averaging Technique for Computing Tangential-Thrust Trajectories," *Journal of Guidance, Control, and Dynamics*, Vol. 28, No. 6, 2005, pp. 1320–1323.

[15] Pouliot, M. R., "CONOPT2: A Rapidly Convergent Constrained Trajectory Optimization Program for TRAJEX," Convair Div., General Dynamics, GDC-SP-82-008, San Diego, CA, Jan. 1982.

[16] Gao, Y., and Kluever, C. A., "An Algorithm for Computing Near Optimal, Many-Revolution Earth-Orbit Transfers," AAS Paper 05-371, 2005.